Theoretical study of the effect of salt and the role of strained hydrogen bonds on the thermal stability of DNA polymers

Y. Z. Chen and E. W. Prohofsky

Department of Physics, Purdue University, West Lafayette, Indiana 47907
(Received 9 June 1993)

In this paper we show that ionic effects on the thermal stability of interbase hydrogen bonds of an infinitely long DNA polymer with repeating sequence can be analyzed at the molecular level of detail using a modified self-consistent phonon formulation of anharmonic lattice dynamics theory. The interactions of the charged groups of DNA with each other and with the diffuse ionic cloud surrounding it in solution are approximately represented in the framework of Soumpasis's potential of mean force between the interacting charge groups [J. Biomol. Struct. Dyn. **6**, 563 (1988); Biopolymers **29**, 1089 (1990)]. The tension from the salt-dependent potential of mean forces and other nonbonded forces across the interbase hydrogen bonds generate a strain in the mean H-bond length. This strain alters the dynamic behavior of these hydrogen bonds. The self-consistently determined bond-disruption probabilities are therefore dependent on the bulk salt concentration. Our calculated premelting interbase-hydrogen-bond-disruption probabilities and the extrapolated melting temperature for a *B*-DNA guanisine-cytosine homopolymer [poly(dG)·poly(dC), i.e., polymer G on one strand of hydrogen bonded to polymer C on the other] are in fair agreement with experimental observations over a wide range of salt concentrations.

PACS number(s): 87.10.+e, 63.20.Dj, 63.70.+h, 87.15.By

I. INTRODUCTION

The stabilizing and destablizing effects of ionic environment on the structure and conformation of the DNA double helix have long been recognized. Earlier studies of DNA thermal denaturation showed a strong dependence of the melting temperature on the nature of the metal ions in solution [1,2]. Other examples are the cooperative DNA helix-helix interconversions in solution such as the $B \rightarrow A$ transition induced by increasing amounts of organic cosolvents [3] and the salt-induced $B \rightarrow Z$ transition [4]. Ionic effects also play a central role at all levels of DNA structural organization [5] and ligand-DNA binding equilibria [6].

A number of polyelectrolyte theories have been formulated to deal with some elements of the ionic effects on DNA. Manning developed a counterion condensation theory (CC theory) of polyelectrolyte [7] and applied the theory to DNA [8]. It has been shown [8] that this theoretical model, when applied to DNA, with the assumption of a relation between the enthalpy difference at the melting temperature and temperature, gives a melting temperature proportional to the logarithm of the salt concentration in agreement with various experimental measurements. Recently progress has been made in the construction of the CC theory based on more realistic polyion charge-distribution models [9]. Many authors have employed the Poisson-Boltzmann (PB) approach [10,11], the hypernetted-chain approximation [12], and Monte Carlo simulation techniques [12,13] to compute the ionic distribution around a highly charged biomolecule modeled as an infinitely long and uniformly charged cylinder. Methods for solving the PB equation for more realistic structural models of DNA have also emerged [14]. Advances have also been made by applying statisti-

cal theories of electrolytes in conjunction with detailed geometry of DNA for the study of salt effects on DNA. This includes the development of a potential of mean-force approach [15,16] and the reference-interacting-site model [17]. Soumpasis and colleagues [15,16] have shown that their potential of mean force (SPMF) approach is particularly useful in describing simple salt effects on DNA structure and structural transitions at higher salt concentrations.

To the best of the authors' knowledge, no microscopic theoretical study other than Manning's simple two-state analysis has been carried out that deals with a fundamental problem of the effect of ionic environment on DNA base-pair stability. It is well known that DNA undergoes fluctuational base-pair opening and bond disruption even at temperatures far below the melting temperatures [18,19]. Premelting base-pair opening can be measured by such experiments as imino proton exchange [19]. The observed open state corresponds to a state in which all of the interbase H bonds in a base pair are disrupted [20,21]. The stability characterized by the bond-disruption probabilities are strongly dependent on the bulk salt concentration particularly in the low-salt regime. At room temperature and at physiological concentrations the measured single base-pair opening probability for a *B*-DNA adenine-thymine (AT) pair is in the range of 10^{-3} to 10^{-5} [19]. The measured probability for a guanine-cylosine (GC) pair is even smaller, which is in the range of 10^{-6}. On the other hand, the low-salt DNA melting measurements [1] show that a natural DNA is denatured at room temperature at $\sim 10^{-4} M$ NaCl depending on the exact GC content.

In an earlier work [22] we have carried out a preliminary study to evaluate salt-dependent DNA bond disruption probabilities at premelting temperatures. In another

work we have also studied the effect of hydrostatic pressure on the melting temperature of DNA [23]. Both works were carried out based on the incorporation of the concept of strained H bonds into a microscopic self-consistent harmonic approach of DNA dynamics. In the present paper we show that this approach can also be used to predict the observed salt-dependent behavior of the melting temperature of DNA.

II. THEORETICAL BASIS

In our earlier studies of DNA we have introduced a modified self-consistent phonon approximation (MSPA) theory to analyze the thermal stability of DNA [20,24]. The theory is a microscopic theory in that the coordinates of the helix are from fiber and crystal data and the room-temperature force constants of the helix are fitted to x-ray and spectral data. All of the interbase H-bond force constants are determined by a MSPA algorithm and are dependent on temperature and environment. They are determined by integrating the second derivative of an interatomic potential weighted by a function that effectively limits the displacement to the proper effective box. In another work we showed that when the cooperative effect of the open base pairs is taken into account, the MSPA-calculated base-pair opening probabilities show typical cooperative transitions at temperatures close to the observed melting temperature [25].

Our model is for a dissociation of an effective double helix, it is not equivalent to the dissociation of a molecule in vacuum. The MSPA calculation implicitly incorporates the stability caused by balancing the static forces associated with expansion from a given conformation. One then ignores the static interactions that led to the stable conformation in the dynamics and deal only with changes in energy caused by departures from that equilibrium. The theory achieves a separation of the static structure or ground-state solution from the dynamic solutions. The elements that implicitly go into the static part of the potential are effects of hydration, solvent, ion cloud, polyelectrolyte effects, etc. If these effects do not change significantly, for example, with temperature, then they are always present but do not enter into the dynamics calculation. The MSPA melting calculation then describes the dynamics leading to H-bond disruption of a system with change in temperature in a particular unchanging static environment that includes all the static stabilizing elements.

Our earlier calculations were limited to physiological salt concentrations that correspond to fiber x-ray studies and fibers used in Raman and ir studies from which our parameters were refined. In particular the positions of the minima of the interbase H-bond Morse potentials were fit to x-ray data. In the logic of the harmonic approximation static salt effects are incorporated into the effective hydrogen-bond Morse potential and it is a correct potential only for salt concentration at which it was fit. We will define this salt concentration as C_0 the nominal salt concentration.

If one changes the environment, such as changing salt concentration, one has altered the static part of the potential that is usually ignored in a harmonic approach

and one has to put back in the effects of such changes to compare the dynamics of the two cases. As shown below this change in the statics of the system can be incorporated into MSPA calculations and we find that it interacts synergistically with the dynamics of the system. We retain the harmonic advantage of not having to solve for the ground-state conformation from scratch. The ground-state-conformation problem is the most difficult and as yet unsatisfactorily solved theoretical problem. This is because the differences in energy between various conformations is less than the accuracy with which the calculations are carried out.

To incorporate the salt-induced change of statics into the MSPA calculation we include the tension from the salt-screened phosphate-phosphate electrostatic and other nonbonded forces across the interbase H bonds. These forces must be compensated for by generating a compensating stress which arises from an induced strain in the mean H-bond length. This stress from the H bonds, which is a static stress, is what keeps the Coulomb repulsion from disrupting the helix. This in turn affects the bond fluctuational motion and vibrational modes of the base pair. The thermal stability of the interbase H bonds are therefore dependent on the strength of the interstrand phosphate-phosphate interaction, and therefore are dependent on the bulk salt concentration. The effect of salt on the base-pair thermal stability can then be determined through the MSPA self-consistent calculations.

III. MSPA PROCEDURE

In MSPA a DNA molecule is described at the atomic level of detail [24,25]. For convenience we treat the hydrogen atoms as if they are rigidly bound to other atoms and their masses are added to these parent atoms. Therefore the dimensionality of the system is that of the heavy atoms in the molecule. In principle we conceive of a DNA helix with all the interatomic interactions represented by realistic bounded potentials. These potentials are then replaced by MSPA self-consistent unbounded harmonic interactions. The effective force constants can be calculated self-consistently at each temperature and in a particular environment.

In DNA not all the effective force constants need to be self-consistently calculated. Some of the force constants change little with temperature and environment and they can be assumed to be independent of temperature and environment. These force constants are refined to experimental data. They include the valence force constants and the long-range nonbonded force constants. Our valence force constants for the bases and the backbones are from Refs. [26] and [27], respectively. In addition to the valence force constants the long-range nonbonded force constants are necessary to reproduce the observed acoustic modes [28] and these force constants are formulated in Refs. [28] and [29]. To further simplify the calculation we assume that the base stacking force constants have the same temperature dependence as that of the average of the interbase H-bond force constants. Therefore only the interbase H-bond force constants need to be calculated in the full MSPA formalism. The force con-

stant for an intact H bond can be given by an integration over the second derivative of a Morse potential weighted by a vibrational distribution function [24]. The Morse potential is used to mimic the real potential between the two end atoms of a H bond. The parameters of this potential for a GC pair used in our cooperative MSPA formalism can be found in Ref. [25]. We point out that even though not all of the force constants need to be calculated, the equations of the motions of the system have to be solved in the full dimensionality of the system.

For an infinitely long DNA polymer with repeating sequence one can further reduce the calculation by utilizing helical symmetry inherent in the sequence. We then divide the DNA helix into unit cells. A unit cell contains a single repeating section which is composed of one or more base pairs and the associated sections of backbones. The normal-mode calculation can then be reduced to a number of calculations each of the dimensionality of a single unit cell.

We have defined [21] an individual bond disruption probability P_{li} and base-pair opening probability P_l^{op} as

$$P_l^{op} = \prod_i P_{li} \equiv \prod_i A_{li} \int_{L_{li}^{max}}^{\infty} dr \exp[-(r-R_{li})^2/2D_{li}] .$$

(1)

Here l and i are the index of base pairs in a unit cell and the index of the interbase H bonds of the lth base pair, respectively. A_{li} is the normalization factor and D_{li} is the mean square vibrational amplitude of a H bond. D_{li} can be calculated given the eigenvalues and eigenvectors of the system and A_{li} can be calculated by using D_{li} [21]. L_{li}^{max} is the maximum separation of the interbase H-bond end atoms before disruption and its value can be found in Ref. [25]. The bond length R_{li} is determined by many factors including thermal expansion, cross bond interactions, and the cooperative effects associated with the constraint enforced by the neighboring pairs. These factors will be analyzed below.

In a mean-field calculation such as MSPA one has to average the effect of disrupted bonds as well as intact bonds to determine the elastic moduli of the system. We found that [25] this can be done by the use of a probability-weighted linear combination of the intact-bond force constant and the disrupted-bond force constant. Disrupted-bond force constant can be regarded as zero, therefore the force constant of an interbase H-bond ϕ_{li} can be given by

$$\phi_{li} = (1 - P_{li})\phi_{li}^{int} ,$$

(2)

where ϕ_{li}^{int} is the force constant for an intact H bond.

Apart from the effect of disrupted bonds, one should also consider additional cooperative effects in DNA. The cooperativity between near-neighbor pairs can strongly influence the stacking interactions. Because of this cooperativity a base pair is constrained to some extent in its motion by the pairs on either side of it. We found that [25] this cooperativity can also be introduced into the stacking force constants by the use of open pair probability weighted linear combination of intact-state force constant and open-state force constants for them. Similarly

the interbase H-bond lengths can also be given by open pair probability weighted linear combination of intact bond lengths and open bond lengths. The base stacking force constant $\phi_{ll'}$ and the mean bond length of an interbase H bond R_{li} can be given by [25]

$$\phi_{ll'}^s = (1 - \sqrt{P_l^{op}P_{l'}^{op}})\phi_{ll'}^{int} ,$$

$$R_{li} = (1 - P_l^{uc})R_{li}^{int} + P_l^{uc}R_{li}^{op} ,$$

(3)

where $P_l^{uc} = (P_{l-1}^{op}P_l^{op}P_{l+1}^{op})^{1/3}$ can be regarded as an unconstrained probability. The geometric mean of P^{op} is used as the weighting functions because it is the simplest function that is appropriate to describe both base stacking and the constraint of a base pair by its neighbor. R_{li}^{op} is the unconstrained open bond end atom distance and it is formulated in Ref. [25]. R_{li}^{int} is the intact bond length. It is determined by various cross-strand interactions and thus is dependent on the bulk salt concentration, which will be discussed in Sec. IV.

Given initial force constants one can solve the equations of motion of the system. The calculated eigenvalues and eigenvectors are the used to compute the D_{li}'s. One can then use these D_{li}'s to calculate bond lengths R_{li} and disruption probabilities P_{li}, etc. They are in turn used to calculate new force constants. This MSPA loop is carried out until self-consistency is reached.

IV. SALT EFFECT ON AN INTACT INTERBASE H BOND

The mean length of a thermally equilibrated intact H bond in a large system depends on two factors. One is static forces exerted on the bond that determine the positions of the interatomic potential minima. The second factor is dynamic, i.e., due to the effects of thermal motion in an asymmetric potential (thermal expansion). For a salt-dependent theory of interbase H-bond stability in DNA both factors are present and synergistically interact.

Nonbonded forces acting between strands of the double helix create a tension which is expressed across the intervening bonds. We separate these forces crossing the interbase H bonds into two categories, those from phosphate-phosphate Coulomb forces (f_p) and those forces normally referred to as stacking forces (f_s) arising from nonbonded interactions other than from phosphate atoms. We define the interstrand nonbonded forces as those arising from one atom in one base pair interacting with another in a neighboring base pair on the other strand. Stacking interactions on the same strand are also important for stability and they are included in our thermal vibration calculations, but these interactions do not contribute to the stress that arises across the interbase H bonds. The cross-strand stacking interaction is dominated by van der Waals interactions. This static stacking force across the interbase H bonds is then

$$f_s(C) = -\frac{1}{2} \sum_{\alpha,\beta} \frac{dV_{VW}(r_{\alpha\beta}^{eq})}{dr} \mathbf{r}_{\alpha\beta}^o \cdot \mathbf{r}_h^o ,$$

(4)

where the double sum runs over the atoms in both of the

bases and the atoms in the appropriate nearest-neighbor bases, and $\mathbf{r}^o_{\alpha\beta}$ is the vector defining the orientation of the displacement between the αth atom in one base and the βth atom in the neighboring interstrand base. The force is a function of salt concentration C because at different salt the distances between atoms may change.

The static force per base pair arising from solvent-averaged interstrand phosphate-phosphate repulsion is calculated from Soumpasis's SPMF approach [16]. We consider the interaction of each of the two phosphates in a base pair with their interstrand counterparts up to ten base pairs away. The calculated forces are projected on to the interbase H-bond direction within the base-pair plane, and the resulting effective static force is given by

$$f_p(C) = -\frac{1}{2} \sum_{j,j'} \frac{dW_{11}(r^{eq}_{jj'})}{dr} \mathbf{r}^o_{jj'} \cdot \mathbf{r}^o_h , \tag{5}$$

where $\mathbf{r}^o_{jj'}$ and $\mathbf{r}^o_h$ are the vectors defining the orientation of the displacement between the jth and j'th phosphate groups and the orientation of the interbase H bond, respectively. W_{11} is the potential of mean force between two anions in a homogeneous 1:1 electrolyte. Its detailed formulation can be found in Ref. [16]. In calculating W_{11} one needs to determine the dielectric constant of the environment. An inspection of the geometry of DNA double helix reveals that the phosphate charge is not completely surrounded by the bulk water. It is on the interface between DNA and surrounding water. A phosphate group interacts with near-neighbor cross-strand counterparts (for a B-DNA up to two base pairs apart) for the most part through the double helix rather than through the water. We therefore use a dielectric constant $\epsilon_{eff} = \sqrt{\epsilon_{DNA}\epsilon_{water}}$ for the interactions between these cross-strand phosphate groups which are less than three base pairs apart. For the other interactions a bulk water dielectric constant is used. The bulk water dielectric constant depends on temperature. This temperature dependence can be formulated using the equations developed by Malmberg and Maryott [30] and by Akerlof and Oshry [31].

At all salt concentrations where the double helix is stable, the static forces are in equilibrium, i.e.,

$$f_s(C) + F_p(C) + f_h(C) = 0 , \tag{6}$$

where $f_h(C)$ is the reaction force in the interbase H bonds and it is calculated from the Morse potential V_{Morse}:

$$f_h(C) \equiv \sum_i^{n_l} f_h^{li}(C)$$

$$= - \sum_i^{n_l} \frac{dV_{Morse}(R_{li})}{dR} \tag{7}$$

in which n_l is the number of interbase H bond per base pair. Here we assume the orientations of all the interbase H bonds in a base pair are roughly the same.

One can define a nominal salt concentration C_0 that corresponds to the condition in which the Raman, ir, and x-ray data were determined. Since the parameters of the

interbase H-bond Morse potentials were fitted to these data the interbase H bonds can be regarded as unstrained at C_0, i.e., all the static forces are canceled and no further static force corrections are necessary in the determination of the equilibrium bond lengths. We will show later than for our calculation $C_0 \approx 0.05M$ NaCl.

At a different salt concentration an additional cross strand force df emerges:

$$df = f_p(C) - f_p(C_0) + f_s(C) - f_s(C_0) . \tag{8}$$

This additional cross-strand static force can be further partitioned among all the interbase H bonds. An individual H bond would then be stressed under a force df_{li}. This stress induces a strain dr^C_{li} in the H bond and it can be calculated by the use of Eqs. (6)–(8):

$$dr^C_{li} = \frac{1}{a_{li}} \ln \frac{\eta_{li}}{1 + \sqrt{(\eta_{li} - 1)^2 - 2df_{li}/a_{li}V^0_{li}}} , \tag{9}$$

where a_{li}, r^0_{li}, and V^0_{li} are Morse parameters and $\eta_{li} = 2\exp[-a_{li}(R^{(C_0)}_{li} - r^0_{li})]$. The detailed expression of df_{li} will be given below.

Our analysis indicates that in the premelting region $dr^C_{li} < 0.2$ Å. Therefore the effect contributed from the terms containing dr^C_{li} can be neglected in calculating $f_p(C)$. Moreover, the variation of the static forces arising from base stacking, when projected onto the interbase H-bond orientation, is relatively small. Thus $f_s(C)$ can be solved self-consistently from Eq. (4) instead of being solved analytically.

The mean length of an impact interbase H bond R^{int}_{li} at a salt concentration C and at a given temperature T can in general be written as

$$R^{int}_{li} = r^0_{li} + dr^C_{li} + dr^T_{li} , \tag{10}$$

where r^0_{li} is the potential minimum and dr^T_{li} is the thermal expansion. This thermal expansion is determined by the following condition on the Morse potential:

$$V_{Morse}(r^0_{li} + dr^T_{li} + \mu_{li}) = V_{Morse}(r^0_{li} + dr^T_{li} - \mu_{li}) . \tag{11}$$

The solution of this equation when substituted into Eq. (10) together with Eq. (9) gives rise to

$$R^{int}_{li} = r^0_{li} + \frac{1}{a_{li}} \ln \left[\frac{\eta_{li}}{1 + \sqrt{(\eta_{li} - 1)^2 - 2df_{li}/a_{li}V^0_{li}}} \right]$$

$$+ \frac{1}{a_{li}} \ln[\cosh\mu_{li}a_{li}] , \tag{12}$$

where a_{li}, r^0_{li}, and V^0_{li} are the Morse parameters, $\eta_{li} = 2\exp\{-a_{li}[R_{li}(C_o) - r^0_{li}]\}$. df_{li} is the change of the static force across the corresponding interbase H bond with respect to the static force at the nominal salt C_0.

Increasing the stretch between base pairs does not affect all the interbase H bonds identically. The amino H bonds (two for a GC pair and one for an AT pair) are in series with a rotational degree of freedom of the amino CN bond. The imino H bond lacks this additional degree of freedom and a strain between base pairs has to be fully experienced across the imino interbase H bond. This

geometrical difference leads to a nonuniform apportioning of the stress between the interbase H bonds. Most of the stress is concentrated on the imino H bond for small Coulomb-induced additional force since torsional coefficients are small and large displacement arises for small variations. Only for large additional interbase force does the stress become distributed across all the interbase H bonds. Our analysis indicates that when the added cross strand force on the lth base pair df_l is relatively small such that $df_l < df_{12}^{max}$, the tension created by this force would not alter the interbase H-bonding configuration to such an extent that the additional degree of freedom of the amino interbase H bonds (rotational freedom of the amino C—N bond) is significantly reduced. Here d_{12}^{max} is defined as the maximum additional static force the imino interbase H bond alone can sustain without being broken and it can be given from Eq. (12) by

$$df_{12}^{max} \equiv \tfrac{1}{2}(\eta_{l2}-1)^2 a_{li} V_{li}^0 .$$ (13)

Because of the additional degree of freedom of the amino interbase H bonds, we can assume that when $df_l \le df_{12}^{max}$ this added force or stress is concentrated on the imino interbase H bond ($i=2$ bond) which has no additional degree of freedom. df_{li} is therefore given as follows: for $df_l \le df_{l2}^{max}$,

$$df_{li}=0 \quad \text{if } i \neq 2 ,$$
$$df_{li}=f_p(C)-f_p(C_0)+f_s(C)-f_s(C_0) \quad \text{if } i=2 .$$ (14)

For $df_l \ge df_{l2}^{max}$ the imino interbase H bond itself can no longer sustain the cross-strand static force. It is likely that this bond would be rapidly disrupted as the static force further increases. As a result the tension created by the cross-strand static force will be shifted onto the amino interbase H bonds.

It is now possible to evaluate the C_0. Since our Morse parameters are refined to data at C_0 and at room temperature, then

$$f_p(C_0)+f_s(C_0)-\frac{dV_{\text{Morse}}(R_{li}^x)}{dR}=0$$ (15)

across bond 2 at 293 K. Here R_{li}^x is the x-ray-determined bond length. $f_p(C_0)$ and $f_s(C_0)$ are calculated using the x-ray-determined coordinates. At $T=0$ the bond is at the Morse potential minimum and Eq. (15) becomes

$$f_p(C_0)+f_s(C_0)=0$$ (16)

at 0 K. We point out that $f_p(C_0)$ is calculated from statistical theory and therefore is a temperature-dependent function. $f_s(C_0)$ is also dependent on temperature because the thermal expansion in the interbase H bonds changes with temperature. The calculated value of C_0 is $\sim 0.05M$ NaCl at room temperature C_0 is uniquely determined by Eq. (15) or Eq. (16). It is not a free parameter that can be adjusted to enhance agreement with observation of the melting temperature.

V. RESULTS AND DISCUSSION

We consider here a B-conformation guanisine-cytosine homopolymer poly(dG)·poly(dC). This polymer is regarded as having an infinite number of base pairs. The coordinates of this homopolymer are from fiber studies and the force constants and Morse parameters for the interbase H bonds are the same as in our previous studies [25]. Our calculation is based on the idealized B structure from fiber x-ray studies. Possible conformation changes occurring from DNA solubility at different salt concentrations are ignored. At high salt concentration poly(dG)·poly(dC) is insoluble [32] and alternating GC DNA's are known to convert to limited aggregates of Z conformation [4]. Therefore our calculation of a B-conformation poly(dG)·poly(dC) at high salt concentration regime should only be regarded as an idealized theoretical model calculation.

A. Analysis of the SPMF static force

Figure 1 shows the calculated cross strand SPMF static force $f_p(C)$ vs NaCl concentration for poly(dG)·poly(dC) at 293 K. At low to intermediate salt concentrations $f_p(C)$ increases monotonically with decreasing salt concentration as ion shielding of the Coulomb force is reduced at low salt concentration. At very low salt concentration $f_p(C)$ becomes insensitive to C, indicating that the SPMF has become a simple Coulomb potential in the
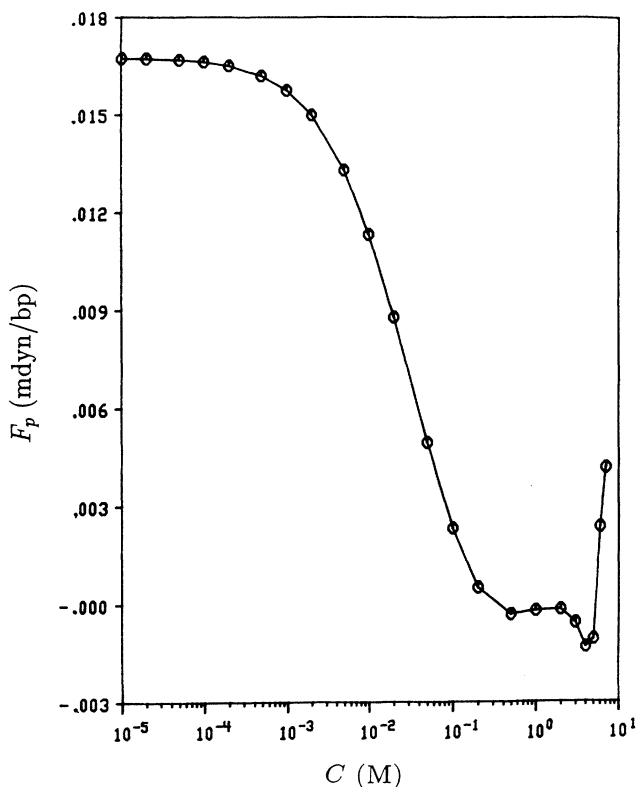

FIG. 1. The calculated cross-strand PMF static force of poly(dG)·poly(dC) vs NaCl concentration. The force f_p is in units of mdyn/bp (1 mdyn = 10^{-8} newton; the abbreviation bp denotes base pair).

low salt limit. At high salt concentration $f_p(C)$ shows a rather complicated salt dependence. We find that below $1M$ NaCl $f_p(C)$ decreases with increasing C. In the range of $1-2M$ NaCl $f_p(C)$ actually becomes an increasing function of salt, although the magnitude of change is very small. When C is further increased, $f_p(C)$ again decreases with increasing C, until C reaches $5M$ NaCl. For $C > 5M$ NaCl $f_p(C)$ increases with C rapidly. The relatively irregular behavior of $f_p(C)$ at high salt concentration is indicative of complex interaction between the ions and underlines the problems of the SPMF in the high salt regime. At high salt concentration Coulomb interactions become unimportant and the SPMF is predominantly determined by the hard-core stacking interactions of the hydrated ions. Earlier SPMF calculation [16] indicates that the high salt hard-sphere interactions are very sensitive to the hard-core distance as well as the hard-core radius. This structure can vary significantly for different assumptions. The calculated SPMF potential shows an oscillating pattern particularly over the distance between 5 and 20 Å. However, it is unlikely that there is much physical significance to this behavior as it is highly model dependent.

Using the results from the MSPA calculation at C_0 we can calculate the value of df_{12}^{max} from Eq. (12). For poly(dG)·poly(dC) we find that $df_{12}^{max} \sim 1.11 \times 10^{-2}$ mdyn. This value corresponds to the potential of mean force at a concentration of $\sim 10^{-3}M$ NaCl as indicated in Fig. 2. Therefore we can conclude that for the particular homopolymer studied the static force df_l can be assumed to concentrate on the imino interbase H bond at salt concentrations greater than $\sim 10^{-3}M$ NaCl. At salt concentrations lower than $\sim 10^{-3}M$ NaCl it is likely that the imino interbase H bond will be disrupted by the cross-strand static force as it further increases. In this region the force is more equitably shared by the amino interbase H bonds.

B. Salt-dependent melting temperature

The melting temperature T_m is defined experimentally as the temperature at which the average of opening probability P_l approaches $\frac{1}{2}$. Figure 2 gives the temperature-dependent profile of the P_l's at several salt concentrations. The calculated P_l's at premelting temperatures are also given in Table I. We find from Fig. 2 that the interbase H bonds of the intact double helix are all disrupted when the temperature increases to a critical point. Near the critical temperature the disruption is highly cooperative, in agreement with experiments. We associate this critical temperature with the melting temperature of the double helix.

The plot of calculated T_m vs salt for poly(dG)·poly(dC) is shown in Fig. 3. In Fig. 3 we also include the available data from experiments on poly(dG)·poly(dC) [2,33] for comparison. The experiments measure an increase in uv absorbance which actually monitors base unstacking. All comparisons of theories of melting, such as the nearest-neighbor helix-coil transition theory, assume a correlation between base unstacking and base-pair separation and we also make this association. We find that our calculated T_m's are in fair agreement with available experimental measurements. In particular the agreement is good for intermediate salt concentrations. As C increases to the high salt region the T_m becomes increasingly flat, the curve actually levels off at around $1M$ NaCl, and even decreases slightly at around $2M$ NaCl. At higher salt concentrations the T_m again increases until the salt concentration reaches $5M$ NaCl where the T_m begins to drop rapidly. Clearly the complicated oscillating behavior of our calculated high salt T_m's is closely related to the complicated salt dependence of the SPMF static force $f_p(C)$ at high salt concentration. This is seen by a comparison between Figs. 1 and 3. Although one does not
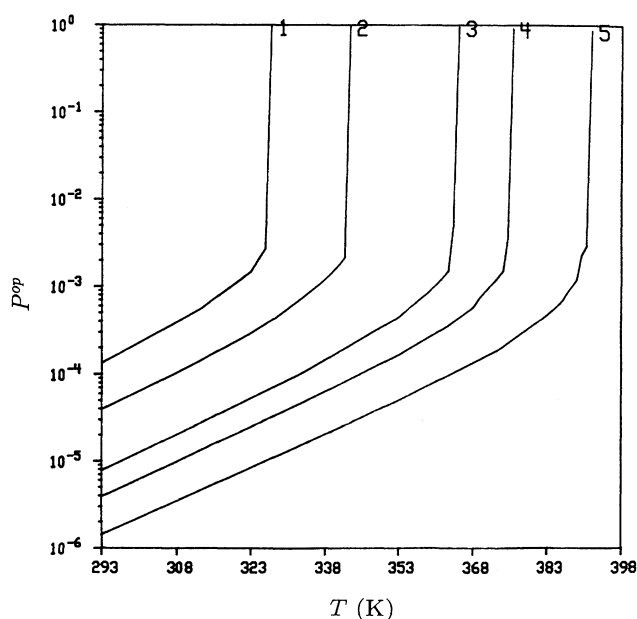

FIG. 2. The calculated base-pair opening probability of poly(dG)·poly(dC) as a function of temperature at several salt concentrations. The assignment of the lines are (1) 0.001 NaCl, (2) 0.01 NaCl, (3) 0.05 NaCl, (4) 0.1 NaCl, and (5) 2.0 NaCl.

TABLE I. Dependence of the premelting base-pair opening probability P^{op} of poly(dG)·poly(dC) on NaCl concentration.

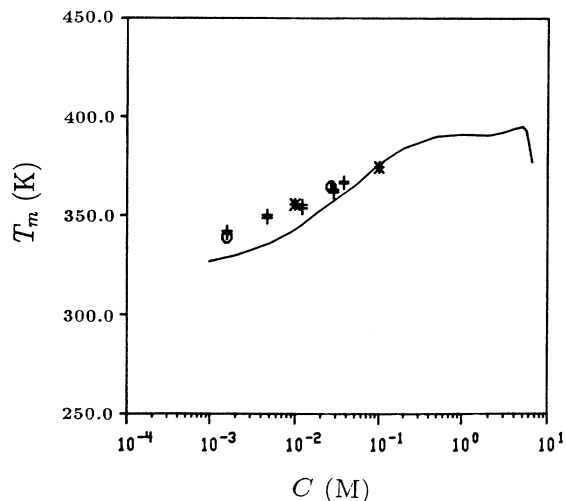| C (M)	P_{op}		
	$T = 293$ K	$T = 313$ K	$T = 353$ K
6.0	1.85×10^{-6}	6.12×10^{-6}	6.78×10^{-5}
5.0	1.04×10^{-6}	3.36×10^{-6}	3.47×10^{-5}
3.0	1.37×10^{-6}	4.45×10^{-6}	4.68×10^{-5}
2.0	1.44×10^{-6}	4.72×10^{-6}	5.02×10^{-5}
1.0	1.39×10^{-6}	4.59×10^{-6}	4.96×10^{-5}
0.5	1.49×10^{-6}	4.98×10^{-6}	5.52×10^{-5}
0.1	3.95×10^{-6}	1.36×10^{-5}	1.67×10^{-4}
0.05	7.91×10^{-6}	2.81×10^{-5}	4.47×10^{-4}
0.0195	2.13×10^{-5}	7.57×10^{-5}	
0.001	4.00×10^{-5}	1.46×10^{-4}	
5.0×10^{-3}	6.78×10^{-5}	2.54×10^{-4}	
1.0×10^{-3}	1.34×10^{-4}	5.63×10^{-4}	

FIG. 3. Calculated T_m of poly(dG)·poly(dC) vs NaCl concentration from this theory (solid line) and the observation from several experiments ($\bigcirc$,$\ddagger$ from Ref. [2] and $*$ from Ref. [37]).

expect this simple model for the SPMF to be particularly accurate at high salt concentrations, our calculation does seem to be in qualitative and, to some extent, quantitative agreement with experiments. The quantitative agreement is significant as no parameters in the theory are fitted to melting data.

Earlier experiments of high salt DNA melting [34,35] showed that as the salt concentration exceeds a certain value the T_m will level off and decrease. The measured turning point of concentration for both a specific form of DNA known as T4 DNA (34% GC pairs) and *M. lysodeikticus* DNA (72% GC pairs) falls in the range between 1.77 and 3.16M NaCl. This is compared to our first turning point of $\sim 2M$ NaCl for poly(dG)·poly(dC). In the region between 2 and 5M NaCl we found an increased T_m and only at salt concentrations higher than 5M NaCl a definitive fall of T_m is observed. The 5M NaCl as the definite turning point predicted by our calculation seems to be at a higher value of salt than seen experimentally. The disagreement is well less than an order of magnitude. The temporary reversal of T_m in the region between 2 and 5M NaCl found in our calculation has not been observed and it is most likely due to the inaccuracy of the

particular SPMF employed in this region.

In the low salt regime our calculated T_m are somewhat lower than the observed T_m for poly(dG)·poly(dC). The lower T_m from our calculation is a result of a condition used in calculating the SPMF static force. The SPMF potential is calculated in the framework of the exponential mean spherical approximation (EXP-MSA) theory. The EXP-MSA radial distribution function used for calculating the charge-dependent part of SPMF potential can only be solved analytically under the condition that the number density of ions is spatially uniform. Although the calculated EXP-MSA radial distribution function indicates a nonuniform ionic distribution around the fixed double-helical array of phosphates, the effect associated with this nonuniform distribution is not fed back into the EXP-MSA formalism. The assumption of a spatially uniform ion number density around DNA, however, is in disagreement with the expected behavior. Manning's work [8] showed that counterions can condense on the surface of DNA. This would lead to a nonuniform ion distribution in the vicinity of DNA. The nonuniform distribution can have a significant impact at a low salt concentration and an accurate analysis for the low salt DNA stability should also take into account the effect associated with the nonuniform ion distribution. Nonetheless our calculation shows that the SPMF in the current form can give a fairly satisfactory result above $\sim 10^{-3}M$ NaCl. The calculated salt dependence of the melting temperature at this salt concentration regime does now show the exact logarithmic curve observed experimentally and predicted by the Manning theory. The calculated curve shows an oscillatory pattern related to the hard-core effects not included in the Manning theory.

We have found no melting-temperature data for poly(dG)·poly(dC) below $10^{-3}M$ NaCl in the literature. Our analysis indicates that the imino interbase H bond will be disrupted quickly as the bulk salt concentration further decreases. This leads to the melting of poly(dG)·poly(dC) at room temperature at salt concentrations below $\sim 10^{-4}M$ NaCl as shown in our earlier calculations [22].

[1] W. F. Dove and N. Davidson, J. Mol. Biol. **5**, 467 (1962).
[2] R. B. Inman and R. L. Baldwin, J. Mol. Biol. **8**, 452 (1964).
[3] V. I. Ivanov, L. E. Minchenkova, E. E. Minyat, M. D. Frank-Kamenetskii, and A. K. Schyolkina, J. Mol. Biol. **87**, 817 (1971).
[4] T. M. Jovin, D. M. Soumpasis, and L. P. McIntosh, Annu. Rev. Phys. Chem. **38**, 521 (1987).
[5] M. T. Record, Jr., S. J. Mazus, P. Melancon, J. H. Roe, S. L. Shanes, and L. Unger, Annu. Rev. Biochem. **50**, 997 (1981).
[6] M. T. Record, Jr., C. F. Anderson, and T. M. Lohman, Q. Rev. Biophys. **11**, 103 (1978).
[7] G. S. Manning, J. Chem. Phys. **51**, 924 (1969).

[8] G. S. Manning, Biopolymers **11**, 937, 951 (1972).
[9] M. O. Fenley, G. S. Manning, and W. K. Olson, Biopolymers **30**, 1191 (1990); **30**, 1205 (1990).
[10] M. Gueron and G. Weisbuch, Biopolymers **19**, 353 (1980).
[11] B. H. Zimm and M. L. Bret, J. Biomol. Struct. Dyn. **1**, 461 (1983).
[12] C. S. Murthy, R. Bacquet, and R. Rossky, J. Phys. Chem. **89**, 701 (1985).
[13] P. Mills, C. F. Anderson, and M. T. Record, Jr., J. Phys. Chem. **89**, 3984 (1985).
[14] B. Jayaram, K. A. Sharp, and B. Honig, Biopolymers **28**, 975 (1989).
[15] D. M. Soumpasis, J. Biomol. Struct. Dyn. **6**, 563 (1988).

[16] R. Klement, D. M. Soumpasis, E. V. Kitzing, and T. M. Jovin, Biopolymers **29**, 1089 (1990).

[17] F. Hirata and R. J. Levy, J. Phys. Chem. **93**, 479 (1989).

[18] H. Teitelbaum and S. W. Englander, J. Mol. Biol. **92**, 55 (1975); **92**, 79 (1975).

[19] M. Gueron, E. Charretier, J. Hagerhorst, M. Kochoyan, J. L. Leroy, and A. Moraillon, in *Structure & Methods, Vol. 3: DNA & RNA,* edited by R. H. Sarma and M. H. Sarma (Adenine, New York, 1990), pp. 113–137.

[20] Y. Z. Chen, Y. Feng, and E. W. Prohofsky, Biopolymers **31**, 139 (1991).

[21] Y. Z. Chen, W. Zhang, and E. W. Prohofsky, Biopolymers **31**, 1273 (1991).

[22] Y. Z. Chen, W. Zhuang, and E. W. Prohofsky, Biopolymers **32**, 1123 (1992).

[23] Y. Z. Chen and E. W. Prohofsky, Phys. Rev. E **47**, 2100 (1993).

[24] Y. Gao, K. V. Devi-Prasad, and E. W. Prohofsky, J. Chem. Phys. **80**, 6291 (1984).

[25] Y. Z. Chen and E. W. Prohofsky, Biopolymers **33**, 351 (1993).

[26] M. Tsuboi, S. Takahashi, and I. Harada, in *Physico-Chemical Properties of Nucleic Acids,* edited by J. Duchesne (Academic, New York, 1973), Vol. 2, pp. 91–145.

[27] K. C. Lu, E. W. Prohofsky, and L. L. Van Zandt, Biopolymers **16**, 2491 (1977).

[28] W. N. Mei, M. Kohli, E. W. Prohofsky, and L. L. Van Zandt, Biopolymers **20**, 833 (1981).

[29] V. V. Prabhu, L. Young, and E. W. Prohofsky, Phys. Rev. B **39**, 5436 (1989).

[30] F. H. Stillinger, in *The Liquid State of Matter: Fluids, Simple and Complex,* edited by E. W. Montroll and J. L. Lebowitz (North-Holland, Amsterdam, 1982), pp. 341–431.

[31] G. C. Akerlof and H. I. Oshry, J. Am. Chem. Soc. **72**, 2844 (1950).

[32] P. A. Mirau and D. R. Kearns, J. Mol. Biol. **177**, 207 (1984).

[33] B. N. Belintsev, A. V. Vologodskii, and M. D. Frank-Kamenetskii, Mol. Biol. (Moscow) **10**, 764 (1976).

[34] K. Hamaguchi and E. P. Geiduschek, J. Am. Chem. Soc. **84**, 1329 (1962).

[35] D. W. Gruenwedel, C. H. Hsu, and D. S. Lu, Biopolymers **10**, 47 (1971).